Journal of Alloys and Compounds 509 (2011) 7168–7174

Contents lists available at ScienceDirect

Journal of Alloys and Compounds

journal homepage: www.elsevier.com/locate/jallcom

Supercapacitor behavior of CuO–PAA hybrid films: Effect of PAA concentration

J.S. Shaikh, R.C. Pawar, N.L. Tarwal, D.S. Patil, P.S. Patil*

Thin Films Materials Laboratory, Department of Physics, Shivaji University, Kolhapur 416004, M.S., India

ARTICLE INFO

Article history:
Received 27 September 2010
Received in revised form 2 April 2011
Accepted 5 April 2011
Available online 12 April 2011

Keywords:
Copper oxide (CuO)
Polyacrylic acid (PAA)
Supercapacitor

ABSTRACT

The Cu–poly(acrylic) acid (PAA) thin films were deposited at room temperature by a simple and cost effective polymer assisted deposition (PAD) method. The solution containing Cu salt and PAA was spin coated to yield the thin films with desired properties. The Cu–PAA films were annealed at 400 °C in ambient air for 4 h to obtain CuO–PAA phase. The effect of PAA concentration on the film properties is studied and characterized by employing various techniques. The structural and surface morphological studies are carried out using X-ray diffraction (XRD) and scanning electron microscope (SEM) respectively. Fourier transform infrared spectroscopy (FT-IR) and FT-Raman spectroscopy are employed to investigate the hybrid film formation. Wetting behavior is studied by measuring the contact angle of water on the film surface. Cyclic voltammetry (CV) studies were carried out to investigate the specific capacitance of CuO–PAA films in aqueous 1 M H_2SO_4 electrolyte. Hybrid films deposited with 2 mM PAA exhibits highest specific capacitance of 65 F g^{-1}.

1. Introduction

Supercapacitor is an active area of research seeking to develop the next generation of cost effective, energy efficient and environmentally–friendly power sources for a variety of day to day applications [1]. Devices based on the supercapacitor are attractive for delivering high energy, long cycle lives, wide range of operation temperature, rapid rate of charging and discharging. They serve as intermediate systems that bridge the power/energy gap between traditional dielectric capacitors (high power) and batteries (high energy) [2]. According to the charge storage mechanism, the supercapacitors are classified into two types: (i) an electrochemical double layer capacitor (EDLC) that stores the energy non-Faradically by the accumulation of the charges at the electrode–electrolyte interface and (ii) redox capacitor that stores the energy Faradically by battery-type oxidation reduction reactions leading to the pseudocapacitive behavior [3]. Various transition metal oxides, such as RuO_2, MnO_2, $Co(OH)_2$, Li_2FeSiO_4, and V_2O_5 have been investigated as possible electrode materials for high-power electrochemical pseudocapacitors [4–8].

Cupric oxide (CuO) is a p-type semiconductor that exhibits narrow band gap (1.2 eV). It is one of the most attractive candidates for supercapacitor electrode materials because of environmental friendliness, low cost and favorable pseudocapacitive characteristics. However, its potential is still not fully explored and some problems need to be addressed. To the best of author's knowledge, there are hardly any reports on CuO thin films, which have been utilized as supercapacitor. Patake et al. reported 32 F g^{-1} capacitance for CuO in 1 M Na_2SO_4 electrolyte [9]. This low specific capacitance is due to neutral electrolyte. One of the reasons for use of neutral electrolyte is the instability of CuO in acidic media. There is no any report on the stability and rate capability of the CuO films. Although CuO is a favorable candidate for supercapacitor application, its relatively low capacity (compared to RuO_2, MnO_2 and IrO_2) inhibits the further developments. To overcome this problem, a new approach should be attempted to improve the specific capacitance by fascinating hybrid CuO–PAA thin films. In view of this, authors have explored the effect of PAA concentration on specific capacitance, rate capability and stability in 1 M H_2SO_4 of CuO–PAA films. Since PAA is hydrophilic, large ionic conductivity, stable in both acidic and basic media and it forms complexes with CuO.

2. Experimental details

All the chemicals (A.R. grade) were used without further purification. The precursor solution for the deposition of hybrid CuO–PAA films was prepared by dissolving 0.2 M cupric chloride ($CuCl_2{\cdot}2H_2O$) in distilled water. The dissociation of $CuCl_2{\cdot}2H_2O$ in water forms Cu^{2+} ions. From this solution, a 10 ml quantity was added with equal amount in three different test tubes. Further the 0.6, 1.4 and 2 mM PAA solution was added. The prepared PAA–Cu solutions were used to deposit films on steel substrates by spin coating. The coated films were dried over night and subjected for annealing at 400 °C for 4 h in air atmosphere. Films are denoted as $CP_{0.6}$ (0.6 mM PAA), $CP_{1.4}$ (1.4 mM PAA) and CP_2 (2 mM PAA).

Thickness of the films is measured using Ambios make surface profiler XP-1 model and found to be ~430, 562 and 680 nm for $CP_{0.6}$, $CP_{1.4}$ and CP_2 films. The structural characterization was carried out using X-ray diffractometer (Philips, PW1710: Almels, Holland) operated at 25 kV, 20 mA with Cu Kα radiation (λ = 1.5406 Å). FT-IR spectrum was recorded on the PerkinElmer, model 783, USA spectrometer to confirm the formation of CuO–PAA hybrid. To record spectrograms pellet was prepared

* Corresponding author. Tel.: +91 231 2609230; fax: +91 231 2691533.
E-mail address: psp_phy@unishivaji.ac.in (P.S. Patil).

0925-8388/$ – see front matter © 2011 Elsevier B.V. All rights reserved.
doi:10.1016/j.jallcom.2011.04.040

by mixing KBr with CuO–PAA powder in 300:1 proportion and then pressing the pellet between two pieces of polished steel. FT-Raman spectroscopy was used to confirm the phase of CuO–PAA. Bruker made (Germany – MultiRAM) with an excitation wavelength (1064 nm) by Nd:YAG source with Ge detector. In this system the Quartz filter is used. The scanning range of FT-Raman is 200–4000 cm^{-1} with resolution 4 cm^{-1}. The surface morphology of the films was examined by using a SEM model JEOL-JSM-6360 Japan, operated at 20 kV. The surface wettability was measured with advanced Goniometer (Model 500-F1, Rame-Hart Instrument Co., USA) at atmospheric pressure and room temperature. CV experiments were conducted at a 20 mV/s using an electrochemical analyzer (CH instruments). The potential was swept between −0.4 and +0.7 V vs. SCE in 1 M H_2SO_4 electrolyte.

3. General strategy adopted for synthesis of hybrid CuO–PAA thin films

Water soluble PAA was used to bind Cu^{2+} ions. Following reactions take place after the addition of PAA in $CuCl_2{\cdot}2H_2O$ solution. The dissociation of the PAA in water:

$$\left[-CH_2-\underset{\displaystyle COOH}{\underset{|}{C}}H-\right]\rightarrow\left[-CH_2-\underset{\displaystyle COO}{\underset{|}{C}}H_2\right]^{-}+H^{+} \quad (1)$$

This reaction can be written as follows:

$$HL \rightarrow L^{-}+H^{+} \quad (2)$$

where H is hydrogen and L is ligand of PAA.

On the basis of modification of Bjerrum model [10], the successive formation of PAA–Cu complexes for divalent Cu^{2+} ions is expressed as follows:

$$HL + Cu^{2+} \leftrightarrow LCu^{+} + H^{+}; b_1 \quad (3)$$

$$HL + LCu^{+} \leftrightarrow L_2Cu + H^{+}; b_2 \quad (4)$$

b_1 and b_2 are the stability constants.

Above reaction explains the formation of L_2Cu due to protonation process.We suggested that two or more ligands of the chelating polymer co-ordinate to a single Cu ion forming complexes such as PAA–Cu (II). From these facts, we presume that more than one ligand of polymers interacts with a single Cu^{2+} to form complexes of LCu^{+} and L_2Cu. Finally, as the protonation process over, the reaction also terminate. The over all reaction becomes as follows:

$$L_2Cu + nHL \leftrightarrow L_2Cu(HL)_n; k_3 \quad (5)$$

where k_3 is the stability constant.

$L_2Cu(HL)_n$ denotes the complex formed this is the final solution used to synthesize the CuO–PAA hybrid thin films.

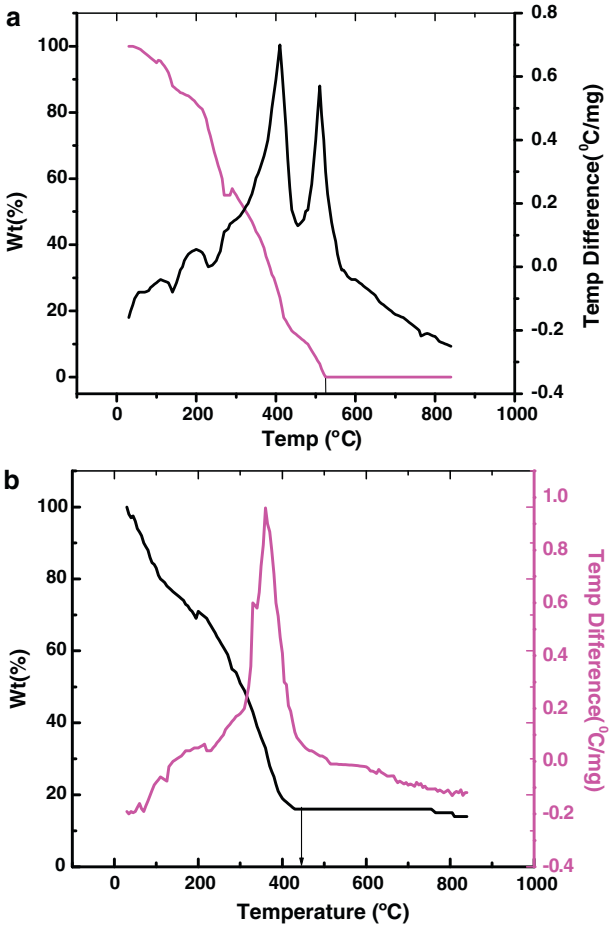

Fig. 1. TGA–DTA curves for (a) PAA and (b) mixture of copper chloride–PAA.

the inflection point coincides with the temperature corresponding to the endotherms and exotherms in DTA trace. The curve exhibits weight losses with increasing temperature. For PAA the weight loss take place in four regions. Region-1 (room temperature to ~200 °C) weight loss is due to desorption of the physisorbed water molecules. Region-II (200–300 °C) weight loss corresponding to decarboxylation. The exotherm begins during the region III (300–500 °C) and is accompanied by the release of H_2O and CO_2.

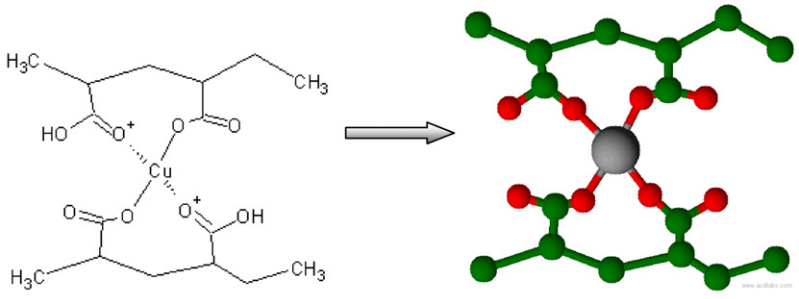

Schematic structure assumed for PAA binding with Cu^{2+} ion by forming PAA divalent Copper complex of $L_2Cu(HL)_n$.

4. Results and discussion

The thermogram recorded for the PAA and mixture of PAA and $CuCl_2{\cdot}2H_2O$ are shown in Fig. 1(a) and (b). The thermal evolution takes place in four consecutive stages with weight losses for which Region IV (500–800 °C) weight loss with exothermic reaction corresponds to release of acrylic acid from depolymerization and CO_2.

For mixture of PAA and $CuCl_2{\cdot}H_2O$, weight losses in three regions with increasing temperature (Fig. 1(b)). Region-I (room temperature to ~90 °C), weight loss is due to desorption of the physisorbed

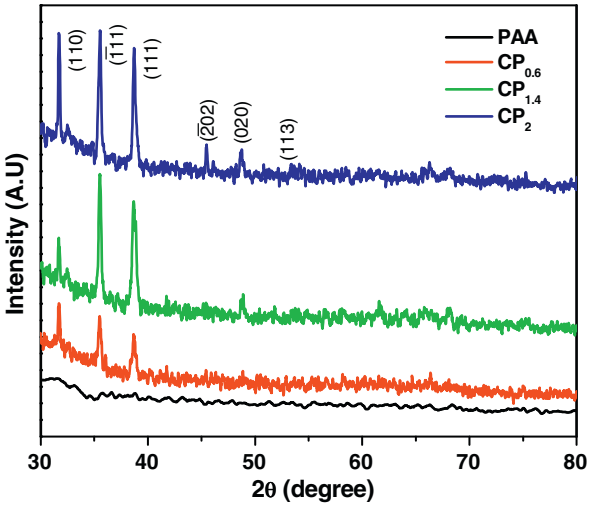

Fig. 2. The X-ray diffraction patterns of $CP_{0.6}$, $CP_{1.4}$ and CP_2 films in the diffracting angle (2θ) range 20–80°.

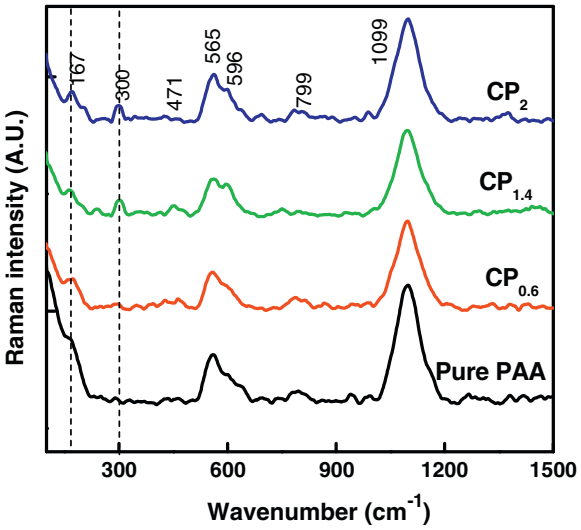

Fig. 4. FT-Raman spectra of the PAA, $CP_{0.6}$, $CP_{1.4}$ and CP_2 films recorded over in the wave number range of 200–4000 cm^{-1}.

water molecules. Region-II (90–450 °C) having exothermic peak, correspond to weight loss decomposition of chlorine and unbonded PAA loss. After 450 °C, the TGA trace is stable with no further weight loss and absence of second exothermic peak (which is observed in PAA due to release CO_2) indicating the formation of thermally stable state of CuO–PAA. Region-III (750–850 °C), a slight weight loss, corresponding to the degradation of PAA from CuO–PAA is observed. Hence PAA may decompose after 450 °C. The FT-IR investigations echo above findings, as well. Chen et al. prepared water soluble MWCNTs by grafting with PAA. They showed that the decomposition of carboxylic groups in pure PAA is lower by 100 °C than that of MWCNTs grafted with PAA. Also, they reported

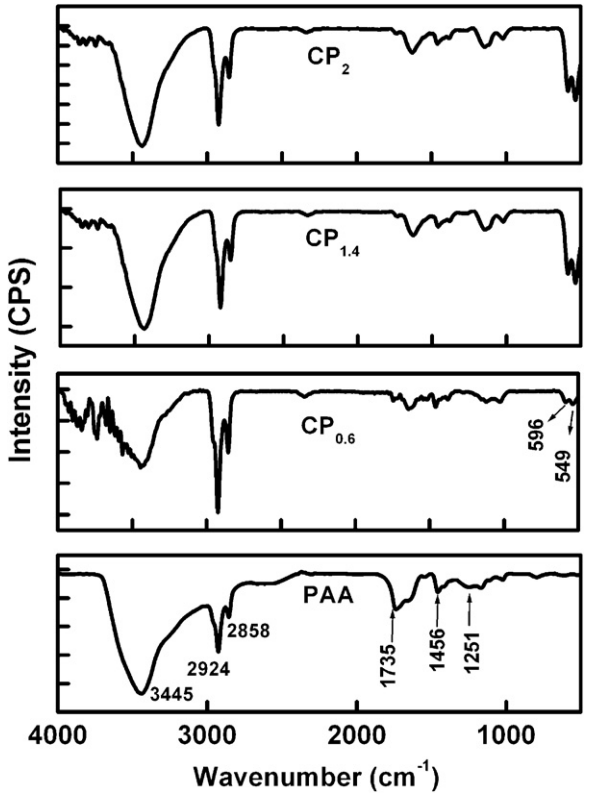

Fig. 3. FT-IR transmittance spectra of the PAA, $CP_{0.6}$, $CP_{1.4}$ and CP_2 films recorded in the wave number range of 500–4000 cm^{-1}.

that all of the functional groups and grafted PAA chains are lost at 800 °C [11].

The structural changes and identification of phases were studied with the XRD technique. The diffracting angle 2θ was varied between 20 and 80° and the patterns of the films $CP_{0.6}$, $CP_{1.4}$ and CP_2 are shown in Fig. 2. The comparison of the observed XRD patterns with the standard JCPDS data (80-0076) confirms the formation of CuO phase with monoclinic crystal structure. The peaks at 35.52°, 38.71°, 48.76°, 53.43°, and 58.27° with d_{hkl} along (1 1 0), ($\bar{1}$ 1 1), (1 1 1), ($\bar{2}$ 0 2) and (0 2 0) planes correspond to CuO. Intensity of all peaks increases gradually with increment in PAA. Thus PAA acts as a crystal growth modifier by helping to grow the crystals in preferred directions [12]. These results are in good agreement with literature [13]. The crystallite's size (t) was deduced from well-known Scherrer's formula:

$$t = \frac{0.9\lambda}{\beta \cos(\theta)} \quad (6)$$

where t = crystallite size in nm, λ = wavelength of X-ray incident on sample, β = full width half maxima and θ = angle at which maximum peak observed. The calculated crystallite sizes are $CP_{0.6}$ = 29 nm, $CP_{1.4}$ = 32 nm and CP_2 = 34 nm.

FT-IR spectra of $CP_{0.6}$, $CP_{1.4}$ and CP_2 films are shown in Fig. 3. The spectrum of PAA is given for comparison. According to the group theory, CuO belong to the C_{2h}^6 space group with two molecules per primitive cell. The degree of vibration freedom represented by

$$\Gamma = 4Au + 5Bu + Ag + 2Bg \quad (7)$$

where Γ is degree of vibrational freedom.

Au, Bu represent infrared (IR) active modes and Ag, Bg represent Raman active modes. Basically, there are six IR active modes (3Au + 3Bu), three acoustic modes (Au + 2Bu) and three Raman

Table 1
Assignments for major FT-IR peaks of CuO–PAA hybrid films.

IR (cm^{-1})	Assignments
3445, 1631	O–H streatching in H–O–H
2853, 2923	C–H band
1744	–C=O stretching of carboxylic group
1461	$-COO^-$ group
1013	C–CH_2 stretching
582	Cu–O stretching along [1 0 1]
536	Cu–O stretching along [1 0 1]

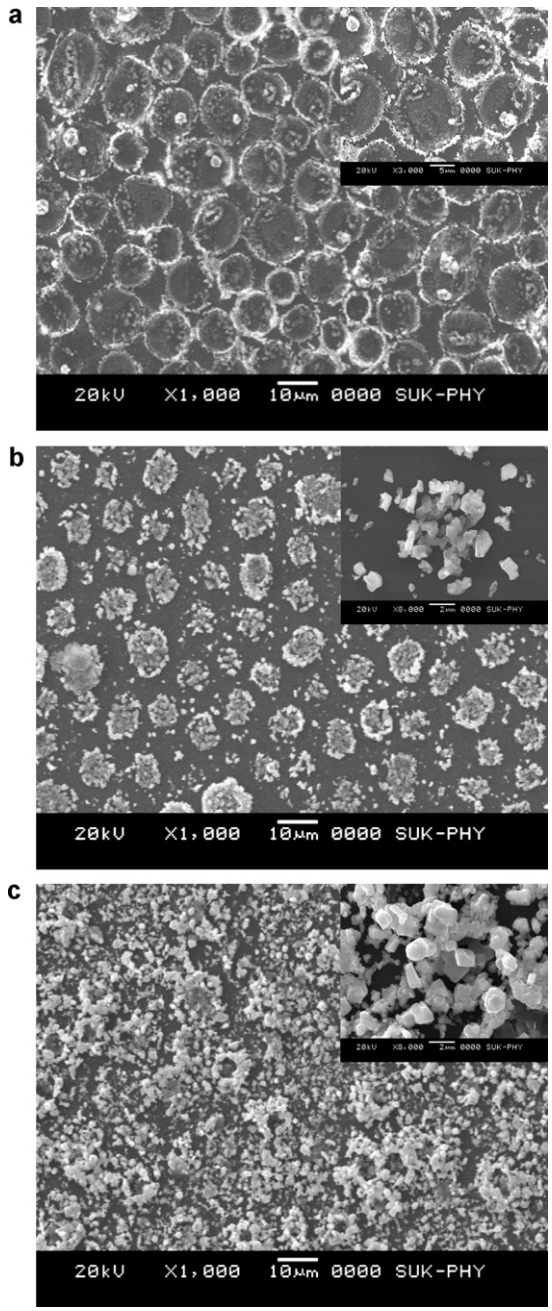

Fig. 5. Scanning electron microscopy images of the $CP_{0.6}$, $CP_{1.4}$ and CP_2 films at 1000× magnifications and inset shows magnified image.

active modes (Ag + 2Bg). FT-IR spectra of the $CP_{0.6}$, $CP_{1.4}$ and CP_2 show the strong twin peak at 536.41 cm^{-1} and 582.58 cm^{-1}. This assigned to the characteristic stretching vibrations of Bu mode in monoclinic CuO. The higher frequency mode at ~582.58 cm^{-1} is attributed to Cu–O stretching along $(\bar{1}\,0\,1)$ direction and modes at ~536.41 cm^{-1} is due to Cu–O stretching along $(1\,0\,1)$ [14]. The prominent CuO twin peaks are observed with increase in concentration of PAA, revels the PAA acts as growth modifier. Hence FT-IR analysis revealed the inorganic component in the sample is a CuO phase with monoclinic crystal structure.

The bands for $CP_{0.6}$, $CP_{1.4}$ and CP_2 films at 3432 and 1631 cm^{-1} correspond to the stretching and bending modes of the hydroxyls of adsorbed water. The peak at 1013, 1461, 1744, 2853 and 2923 cm^{-1} corresponds to PAA by comparing with FT-IR spectrum of PAA and the assignments for major IR peaks are given in Table 1. The peak observed at 1112 cm^{-1} has lower wave number about 20 cm^{-1} comparing to the FT-IR spectrum of PAA suggesting the formation of chemical bond between PAA and the inorganic components [15,16]. The observed peaks cannot be assigned to any decomposition product of PAA like acrylic acid. The peaks of C=C at 1637 cm^{-1}, $=CH_2$ at 984 cm^{-1}, O–H out of plane bend groups at 920 cm^{-1}, C–OH at 1430 cm^{-1}, C–O stretching intense doublet at ~1260 cm^{-1}, and O–H out-of-plane peak at 920 cm^{-1} are absent in the spectra, indicating the absence of acrylic acid in the film [17]. Hence FT-IR spectra revealed the presence of CuO and PAA in films.

FT-Raman spectra of $CP_{0.6}$, $CP_{1.4}$, CP_2 and PAA films are shown in Fig. 4. Three Raman active modes are observed at about 167 (Ag), 300 (Bg) and 596 cm^{-1} (Bg) correspond to Cu–O stretching. The band at about 1099 cm^{-1} is assigned to multi-phonon transition. The peak observed at 1273 cm^{-1} is assigned to CH_2 twisting. The peak at 1402 cm^{-1} corresponds to CH_2 deformation and the peak observed at 1698 cm^{-1} assigned to C=O stretching [12]. Some peaks in PAA are matched with CuO. Blue shift in wave number of Ag and Bg with increasing concentration of PAA are observed. This is due to the chemical bonding between CuO and PAA. FT-Raman studies confirmed the CuO–PAA phase formation.

Fig. 5(a)–(c) shows the SEM micrographs of $CP_{0.6}$, $CP_{1.4}$ and CP_2 films. Periodic structures of CuO–PAA circles are formed for $CP_{0.6}$. As the PAA concentration increased from 0.6 to 1.4 mM, the circle like structures disturbed. Hence porosity of the film is large for higher concentration of PAA. This structure is beneficial for supercapacitor, because it creates penetration path for ion transportation in bulk of the film and reduces the diffusion resistance of the electrolyte into electrode.

Finally, these circles are merged in to the well-distributed faceted crystals for CP_2 film. Hence, the PAA plays a major role in modifying the surface morphology of hybrid films.

Wettability study is important in supercapacitor application. The hydrophilic films are favorable for superior performance of

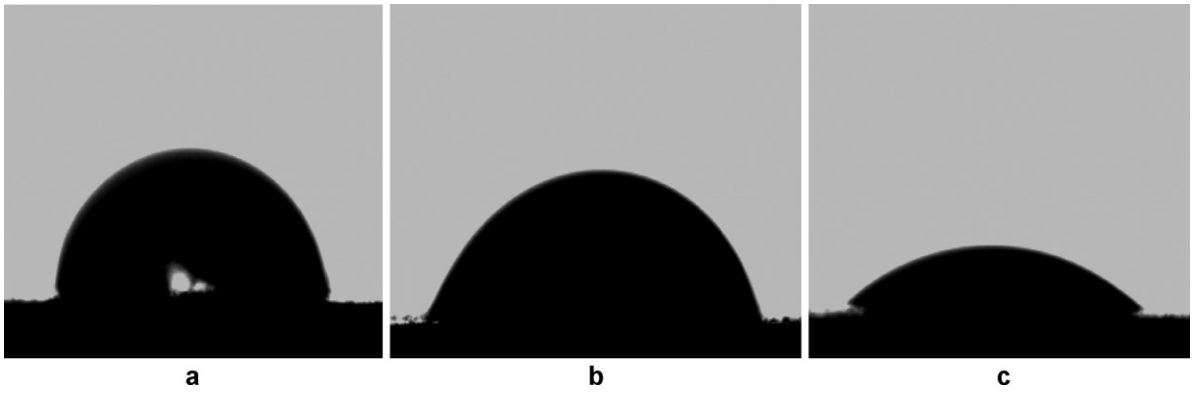

Fig. 6. Contact angles of water droplet on the surface of (a) $CP_{0.6}$, (b) $CP_{1.4}$ and (c) CP_2 films measured with Goniometer at atmospheric pressure and room temperature.

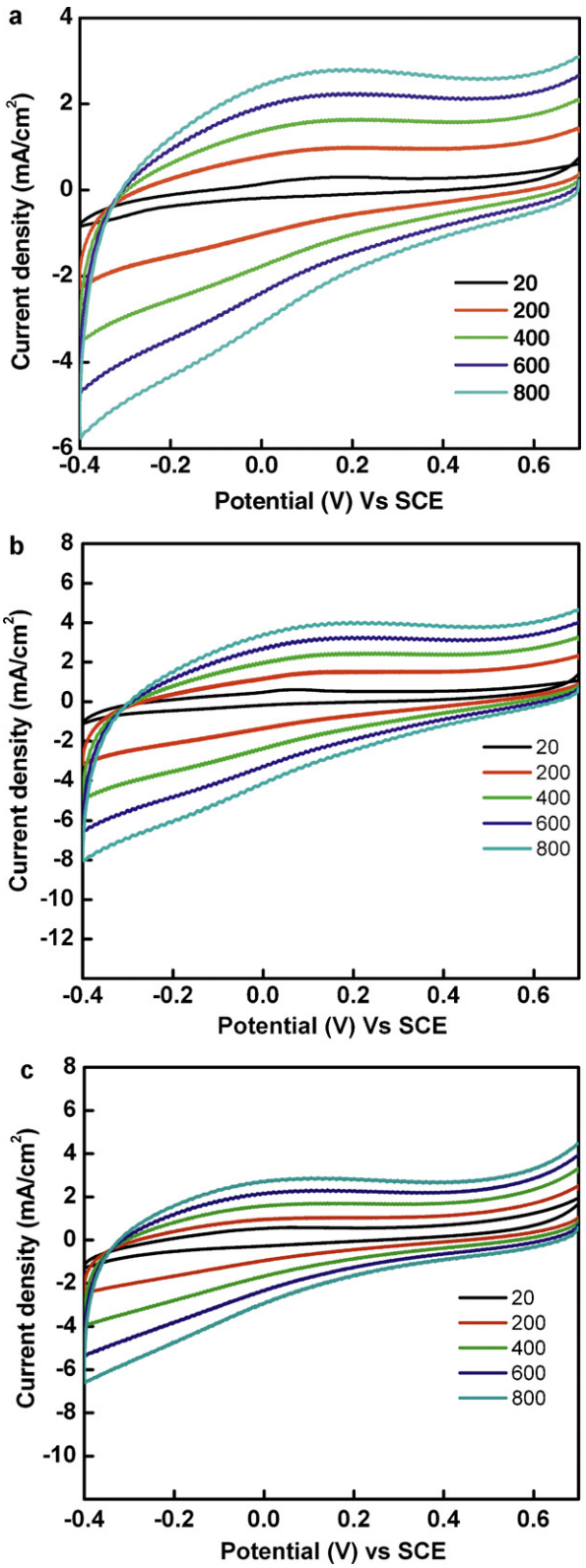

Fig. 7. CVs at different scan rate within a potential window of −0.4 to 0.7 V vs. SCE recorded in 1 M H_2SO_4 for (a) $CP_{0.6}$, (b) $CP_{1.4}$ and (c) CP_2 films.

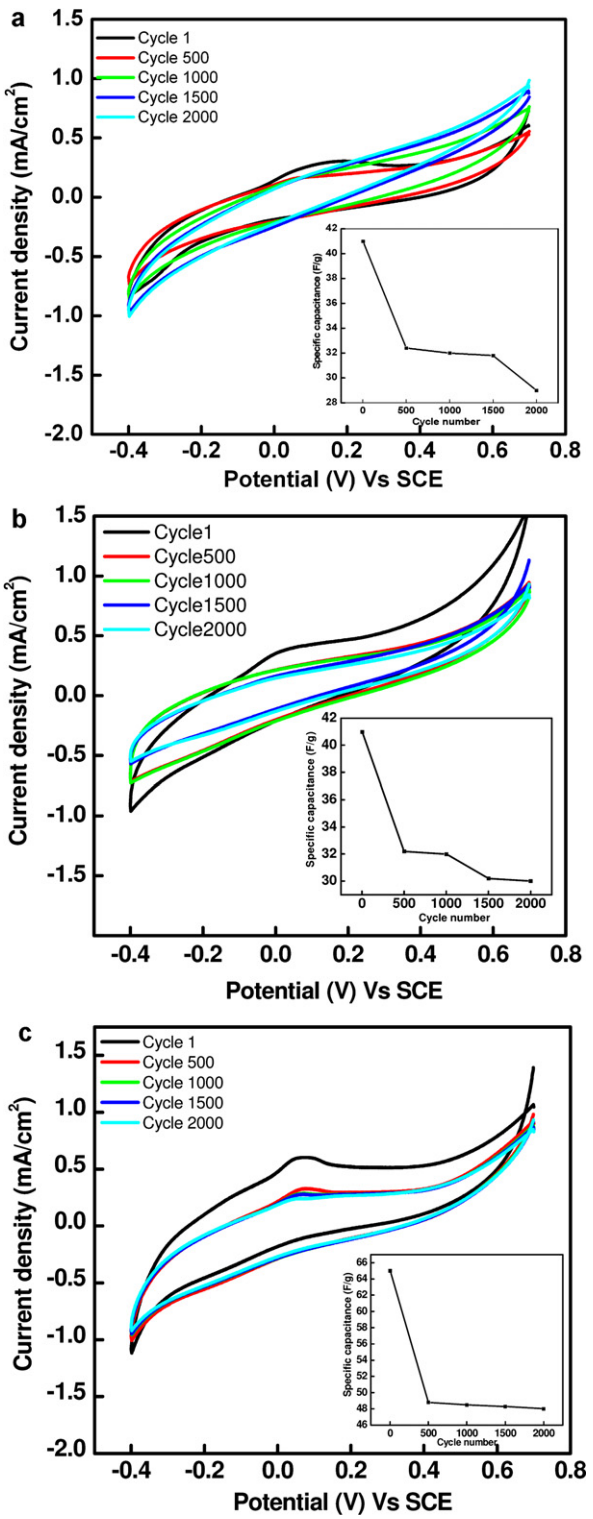

Fig. 8. CVs up to the 2000th cycle at 20 mV/s within a potential window of −0.4 to 0.7 V vs. SCE recorded in 1 M H_2SO_4 for (a) $CP_{0.6}$, (b) $CP_{1.4}$ and (c) CP_2 films.

supercapacitor. The water contact angle photographs of water on the $CP_{0.6}$, $CP_{1.4}$ and CP_2 films are shown in Fig. 6(a)–(c). The contact angle 50, 45 and 42° are observed for $CP_{0.6}$, $CP_{1.4}$ and CP_2 films, respectively. As the PAA concentration increases, the film becomes more hydrophilic. The improvement in hydrophilicity is attributed to the carboxyl group of PAA. Moreover the hydrophilic films are beneficial for supercapacitor because of reduction in the diffusion resistance of the electrolyte into the electrode surface [18].

Cyclic voltammetry (CV) is employed to deduce the pseudocapacitance in aqueous 1 M H_2SO_4 electrolyte, in a conventional three electrode arrangement of following configuration:

SS/CuO–PAA/1 M$H_2SO_{4(aq)}$/SCE/G

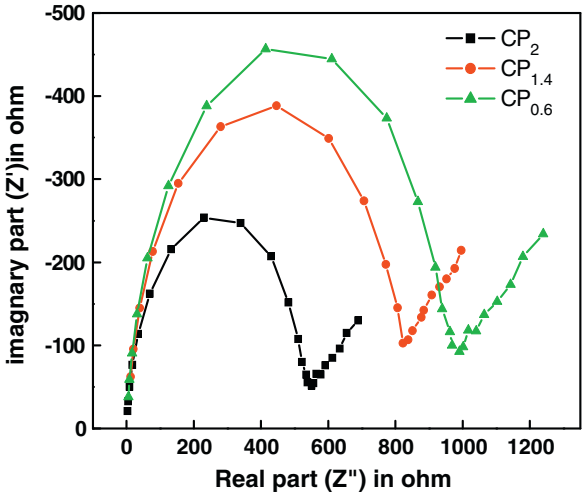

Fig. 9. Niquist plots for $CP_{0.6}$, $CP_{1.4}$ and CP_2 films as the electrode materials.

Hybrid films $CP_{0.6}$, $CP_{1.4}$ and CP_2 are used as working electrodes, saturated calomel electrode (SCE) serving as a reference electrode to which all measured voltage were referred and G is the graphite as a counter electrode.

Two mechanisms/models are proposed for supercapacitor charge storage in CuO. The first mechanism is based on the intercalation/extraction of protons in the electrode that is oxidation/reduction of the electrode (reaction (1) in Eq. (9)), and the surface adsorption and desorption of protons (reaction (2) in Eq. (10)): When the CuO electrode is swept towards negative potential vs. SCE, the cathodic current flows owing to $Cu^{2+} \leftrightarrow Cu^{1+}$ reduction process. Similarly, during positive potential, anodic current flows due to $Cu^{1+} \leftrightarrow Cu^{1+}$ oxidation process. The following reaction represents the redox reaction in the cell:

$$Cu^{2+} + e^- \leftrightarrow Cu^+ \quad (8)$$

$$2CuO + 2H^+ + 2e^- \rightleftharpoons Cu_2O(OH) \quad (9)$$

The charge storage mechanism of CuO electrode in aqueous 1 M H_2SO_4 electrolyte has been proposed as follows:

$$(2CuO)_{surface} + 2H^+ + 2e^- \rightleftharpoons (Cu_2O(OH))_{surface} \quad (10)$$

To evaluate the effect of scan rate (rate capability) on supercapacitor, the CVs at different scan rate were recorded and are shown in Fig. 7(a)–(c) for $CP_{0.6}$, $CP_{1.4}$ and CP_2 films. The average specific capacitance is calculated according to the following equation:

$$C = \frac{i}{V \times W} \quad (11)$$

where i, V and W represent the average current, scan rate and weight of deposited materials. The specific capacitance 32, 41 and 65 F g^{-1} are calculated for $CP_{0.6}$, $CP_{1.4}$ and CP_2 films respectively at 20 mV/s. The increments in specific capacitance with increase in concentration of PAA are due to the increase in wettability, porosity and ionic conductivity of the electrode. Besides, the currents increase with the increase of the scan rate, indicating rapid reversible redox reaction occurred among the electrode materials [18,19].

The stability of an electrode material is important for supercapacitor. Fig. 8(a)–(c) shows CVs of $CP_{0.6}$, $CP_{1.4}$ and CP_2 films up to the 2000th cycle at 20 mV/s. The inset shows the variation of the specific capacitance as a function of CV cycle number. For $CP_{0.6}$ film the specific capacitance decreases up to 2000th cycle. The $CP_{1.4}$ film shows decrease in specific capacitance up to 1500th cycle, further no decrement in specific capacitance (up to 2000th cycle) is observed. We see that in CP_2 film, the specific capacitance value remain stable from 500th cycle (up to 2000th cycle). Hence it is relatively stable than $CP_{0.6}$ and $CP_{1.4}$ films.

Electrochemical impedance spectroscopy (EIS) has been used to investigate the performance of supercapacitor. Fig. 9 shows the relation between Z'' (imaginary) and Z' (real) impedance components (Niquist plots) of $CP_{0.6}$, $CP_{1.4}$ and CP_2 films as the electrode materials. An equivalent circuit shown as below was proposed to fit the spectra. The equivalent circuit is a composed of a solution resistor R_s, a double layer capacitor C_{dl}, a finite-length Warburg diffusion element Z_W, a CuO–electrolyte interface charge resistor R_{ct}, and a faradic pseudocapacitor C_F. The electrochemical processes and mass transfer occurring within the pores and at the CuO–PAA hybrid–electrolyte interface were characterized as a composite interfacial impedance consisting of C_{dl} in parallel with a serial combination of Z_W and R_{ct}. The arrangement of R_F with Z_W in parallel with the C_{dl} is called the "Randles circuit". The equivalent circuit was then completed by putting this composite interfacial impedance in series with R_s and C_F.

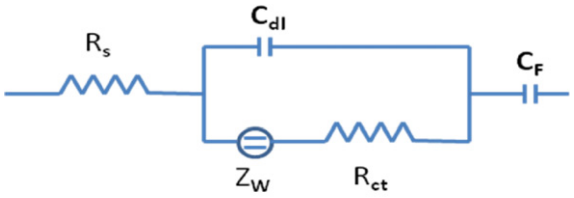

Equivalent circuit of EIS spectra

The Niquist plots of all films consist of a semicircle at high frequency and a line with a slope close to 45° at low frequency region as expected for pseudocapacitor. Semicircle in the high frequency region describing the electron series resistance (ESR) or charge transfer resistance across the electrode/electrolyte interface [20–22]. Also, it evident that the appreciable contribution of the composite interfacial element. However, the Niquist plot of CP_2 has a small semicircle at high frequency region contrast to $CP_{0.6}$ and CP_2 films. Hence CP_2 film has low resistance at the interface of electrode/electrolyte due to hydrophilicity and conductivity of the film.

5. Conclusions

Hybrid CuO–PAA thin films were successfully synthesized by a simple and cost effective PAD method. The effect of PAA concentration on the wettability and supercapacitor behavior of hybrid films has been studied systematically. The morphological transformation from periodic circles to faceted crystals is observed. Films become more hydrophilic as the PAA concentration increased. The deposited films are stable in an acidic media and good rate capability up to 800 mV/s. The specific capacitance increases systematically with the increase in PAA. The increments in the specific capacitance with increase in the concentration of PAA are due to the combined effect of increment in the wettability, porosity and ionic conductivity. The highest specific capacitance of 65 F g^{-1} is observed for 2 mM PAA.

Acknowledgement

The authors are thankful to University Grants Commission, New Delhi, for the financial support through project F. No. 36-211/2008(SR) and the UGC-DSA–I (2010-2015) programs.

References

[1] A. Chidembo, K. Ozoemena, B. Agboola, V. Gupta, G. Wildgoose, R. Compton, Energy Environ. Sci. 3 (2010) 228–236.

[2] X. Liu, P. Pickup, Energy Environ. Sci. 1 (2008) 494–500.
[3] T. Xue, C. Xu, D. Zhao, X. Li, H. Li, J. Power Sources 164 (2007) 953–958.
[4] Y.C. Su, C.A. Chen, Y.M. Chen, Y.S. Huang, K.Y. Lee, K.K. Tiong, J. Alloys Compd. 509 (2011) 2011–2015.
[5] D.L. Fang, B.C. Wu, A.Q. Mao, Y. Yan, C.H. Zheng, J. Alloys Compd. 507 (2010) 526–530.
[6] X. Nia, H. Zheng, X. Xiao, X. Jin, G. Liao, J. Alloys Compd. 484 (2009) 467–471.
[7] K. Karthikeyan, V. Aravindan, S.B. Lee, I.C. Jang, H.H. Lim, G.J. Park, M. Yoshioc, Y.S. Lee, J. Alloys Compd. 504 (2010) 224–227.
[8] L.M. Chena, Q.Y. Lai, Y.J. Hao, Y. Zhao, X.Y. Jic, J. Alloys Compd. 467 (2009) 465–471.
[9] V. Patake, S. Joshi, C. Lokhande, O. Joo, Mater. Chem. Phys. 114 (2008) 6–9.
[10] T. Tomida, K. Hamaguchi, S. Tunashima, M. Katoh, S. Masuda, Ind. Eng. Chem. Res. 40 (2001) 3557–3562.
[11] S. Chen, G. Wu, Y. Liu, D. Long, Macromolecules 39 (2006) 330–334.
[12] J. Dong, Y. Ozaki, K. Nakashima, Macromolecules 30 (1997) 1111–1117.
[13] G. Zou, H. Li, D. Zhang, K. Xiong, C. Dong, Y. Qian, J. Phys. Chem. B 110 (2006) 1632–1637.
[14] Y. Xu, D. Chen, X. Jiao, J. Phys. Chem. B 109 (2005) 13561–13566.
[15] V.I. Chegel, O.A. Raitman, O. Lioubashevski, Y. Shirhov, E. Katz, I. Willner, Adv. Mater. 14 (2002) 1546–1549.
[16] J. Wu, Q. Tang, H. Sun, J. Lin, H. Ao, M. Huang, Y. Huang, Langmuir 24 (2008) 4800–4805.
[17] L.J. Ward, W.C.E. Schofield, J.P.S. Badyal, Chem. Mater. 15 (2003) 1466–1469.
[18] B.E. Conway, Electrochemical Supercapacitor: Scientific Fundamentals and Technological Application, Kluwer Academic/Plenum Publisher, New York, 1999.
[19] Y. Li, K. Huang, S. Liu, Z. Yao, S. Zhuang, J. Solid State Electrochem., doi:10.1007/s10008-010-1128-3.
[20] A.T. Chidembo, K.I. Ozoemena, B.O. Agboola, V. Gupta, G.G. Wildgoose, R.G. Compton, Energy Environ. Sci., doi:10.1039/b915920g.
[21] Y. Li, H. Xie, J. Wang, J. Solid State Electrochem., doi:10.1007/s10008-010-1150-5.
[22] G. Sun, K. Li, Y. Liu, J. Wang, H. He, J. Wang, J. Gu, Y. Li, J. Solid State Electrochem., doi:10.1007/s 10008-010r-r1129-2.